

# FEM STRUCTURAL ANALYSIS FROM UAV PHOTOGRAMMETRY PROJECTS. CASE STUDY: TWENTY EYES AQUEDUCT IN THE WADI OF CARCAUZ (ALMERIA, SPAIN)

**José Manuel Casimiro-Bernárdez**

HL Estructuras, Plaza de los Campos, Granada

**Patricio Martínez-Carricondo\*, Francisco Agüera-Vega, Fernando Carvajal-Ramírez**

Department of Engineering, University of Almería (Agrifood Campus of International Excellence, ceiA3/ Peripheral Service of Research and Development Based on Drones), Spain

*Keywords:* UAV photogrammetry, HBIM, FEM, structural simulation, cultural heritage

## 1. Introduction

The traditional approach to structural modelling and simulation of historical constructions presents numerous difficulties, such as the acquisition of geometric data in the field, the accuracy of the resulting 3D models or the oversimplification of the structural models due to the geometric complexity of the work under study. However, the task of reconstructing, protecting and conserving our heritage has been significantly facilitated by recent advancements in photogrammetry, which relies on images captured by Unmanned Aerial Vehicles (UAVs). These advancements also encompass the development of integrated Building Information Modelling (BIM) models and the enhancement of computational performance in modern computers for simulating the structural behaviour of complex constructions [1-2]. With the growing popularity of UAVs, commonly known as drones, fields such as engineering and architecture have leveraged the opportunity to achieve a high degree of accuracy in the information collected through photogrammetric flights with UAVs and to address the limitations of traditional technology for reconstructing buildings or civil works that constitute our historical heritage [3]. Similarly, the significant progress made in computers and software facilitating three-dimensional (3D) modelling has provided an ideal platform for the virtual reconstruction, conservation and public exhibition of our cultural heritage [4-9].

Since the beginning of the 21st century, significant advancements have taken place in Terrestrial Laser Scanners (TLS) [10] and UAV photogrammetry [11], greatly facilitating the generation of 3D models. Thanks to the combination of modern computers and photogrammetry [12], it is now possible to use photos taken at various heights and angles to create 3D models based on point clouds derived from these images.

This process can be accomplished using a variety of computer programs, even when photos are captured using traditional cameras. This transformation is enabled by a cost-effective method called Structure from Motion (SfM), developed in computer

---

\* Corresponding author: pmartinez@ual.es

vision, which can convert a series of images taken from different angles into a 3D representation [13]. The SfM algorithm generates a point cloud representing the object under study, along with the position and orientation of the camera photographs. SfM incorporates stereoscopic techniques from various views (Multiview Stereo Matching) [14], which produce a 3D structure through the overlap between photographs taken from multiple locations and angles, related by means of a Scale Invariant Shape Transformation and bundle adjustment. Following this algorithm's processing, a point cloud is obtained without scale and in relative coordinates, typically requiring georeferencing with an official reference system, either through direct methods using geolocation data from photographs or indirect methods using Ground Control Points (GCP) [15]. According to various studies, the results obtained through the SfM algorithm provide 3D information with similar accuracies to those obtained through TLS [16-17]. The morphology and accessibility of the feature or study area define the most suitable technique: TLS or UAV photogrammetry [18]. Indeed, one of the primary challenges of TLS is inaccessible areas. In such cases, UAVs efficiently and economically facilitate data collection [19-20]. In addition, a straightforward approach to enhancing results obtained with SfM photogrammetry is by using oblique photographs, enabling the visualisation of details that may remain hidden in plain view images, without the need for ground photographs [21-22]. However, there may also be accessibility challenges for UAVs in small geometries, such as long, narrow corridors.

The development of the BIM model commences with the availability of the dense point cloud or 3D mesh of the complex under study, along with CAD files, other design materials or using in-situ measurements.

BIM allows for the collaborative creation and management of a building or civil engineering project throughout its life cycle. Its aim is to reduce time and resources in asset design, development and management, while minimising errors by centralising all project information into a digital model produced by all stakeholders [23]. BIM represents an evolution from traditional plan-based design systems, as it incorporates geometric (3D), time (4D), cost (5D), environmental (6D) and maintenance (7D) information [24]. Another crucial aspect of BIM is its interoperability, facilitating information sharing among all project entities (Construction Operations Building Information Exchange). Although BIM methodology has been primarily used in the construction sector since the turn of the century [25], it has recently gained momentum in historical heritage management and documentation [26-27]. When applying BIM methodology to digitise existing information about artistic or historical works of heritage value, it is referred to as Historic Building Information Modelling (HBIM). This term was initially coined by Professor Maurice Murphy of the Dublin Institute of Technology [28]. The primary goal of HBIM is to obtain BIM models of existing buildings, modelled from parametric objects containing various types of information that can be easily updated, replaced or aggregated. The implementation of HBIM undoubtedly facilitates the dissemination of built heritage. However, since each building is unique and may have anomalies in morphology and constituent materials, the application of this methodology to historical reconstruction depends on the specifics of each building. For the creation of these models, historical information on the building, in addition to data provided by TLS or photogrammetry for model digitisation, is of great assistance. This process, known as 'Cloud-to-BIM' or 'Scan-to-BIM', allows for the realistic reconstruction and visualisation of the modelled building [29-32]. The quality of the model will be related to the level of detail aimed for during the modelling phase. In the case of heritage elements in a dilapidated state, this level will also depend on the existing information on geometry and other original features. The ability to employ Finite Element Models (FEM) to replicate the structural behaviour of buildings is one of the primary challenges currently confronting the

3D digital modelling of our heritage. ‘BIM-to-FEM’ refers to the process of converting a BIM or HBIM into a structural FEM [33-34]. Indeed, with the increasing development of interoperability between BIM models, the same model can serve multiple purposes, with structural analysis being one of them. Specific BIM plugins exist for generating FEMs, such as CSiXRevit. Although exchanging information between a 3D architectural model and its corresponding FEM may appear straightforward, when dealing with complex geometries, the current software interoperability does not always allow for discretisations compatible with elements readable by the main calculation programs (Staad.Pro, SAP2000, SOFiSTiK, Robot, etc.). Therefore, it is crucial that from the outset of the modelling phase the analyst considers not only the accurate reproduction of the assembly but also the fulfilment of the requirements necessary for generating a correct FEM, distinguishing between small irregularities and complexities that may influence structural behaviour and those that are inconsequential [35].

The aim of this project is to develop an HBIM of the Twenty Eyes Aqueduct (Acueducto de los Veinte Ojos) in the wadi of Carcauz, situated between the municipalities of Felix and V́icar (Almería), using a point cloud acquired through UAV photogrammetry. This endeavour will enable a thorough analysis of the aqueduct’s structural behaviour and serve as a starting point for future research into recovery and conservation strategies. This process is summarised in the innovative two-step methodology termed Cloud-to-BIM-to-FEM.

## 2. Materials and methods

The methodology employed in this study is founded on the examination of historical data and the precise location of the Carcauz Aqueduct. Additionally, a survey of the current condition of the aqueduct was devised, accomplished through UAV photogrammetry. Using this data, an HBIM of the heritage structure was generated, employing specific software for processing photogrammetric data (Agisoft Metashape) and for designing the HBIM (Autodesk Revit 2022). The accuracy of the BIM model was verified using geometric validation software (CloudCompare). Finally, the 3D geometry of the BIM model was converted into shell elements (2D finite elements) compatible with the software used for structural analysis (SAP2000), wherein the structural behaviour of the aqueduct is assessed. The workflow employed for the creation of this document is outlined in Figure 1.

### 2.1. Study site

The Carcauz Aqueduct is a hydraulic structure stretching approximately 3.2 km along the slopes of the Carcauz-Casablanca wadi. Situated on the southern slopes of the Sierra de Gádor in southeastern Spain, it lies within the province of Almería, bordering the municipalities of V́icar and Felix [36].

This study focuses on the Twenty Eyes Aqueduct, a component of the hydraulic complex mentioned above, as depicted in Figure 2. The coordinates in UTM projection, Huso 30 N and ETRS89 datum for the location of the aqueduct are as follows:

- Southwest (526.450, 4.075.645)
- Northeast (526.470, 4.075.688)

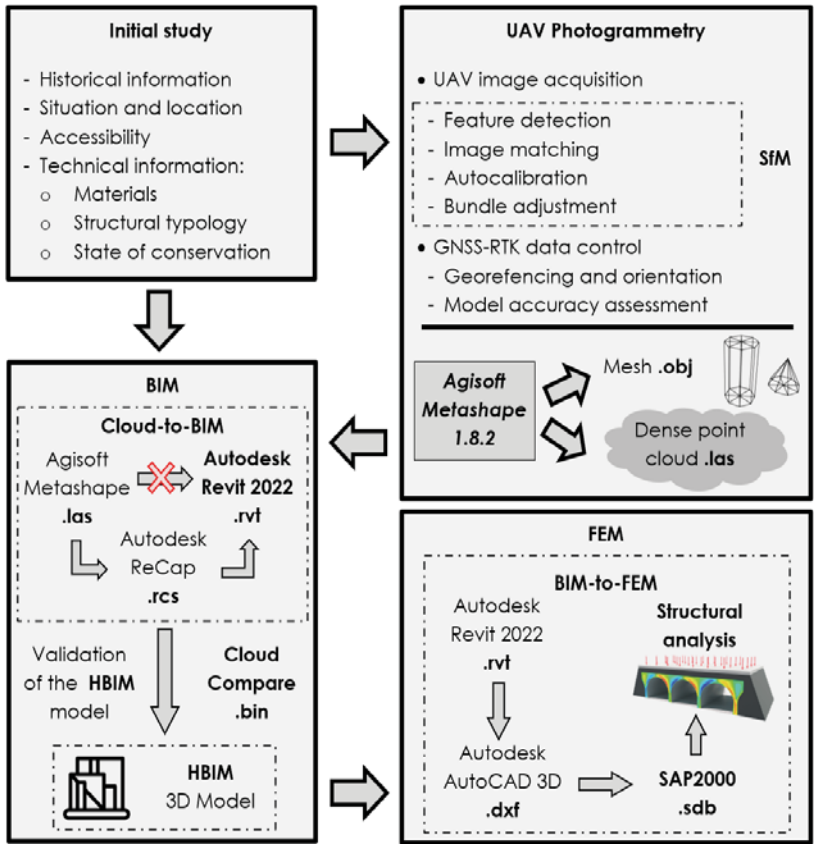


Figure 1. Workflow implemented in this study.

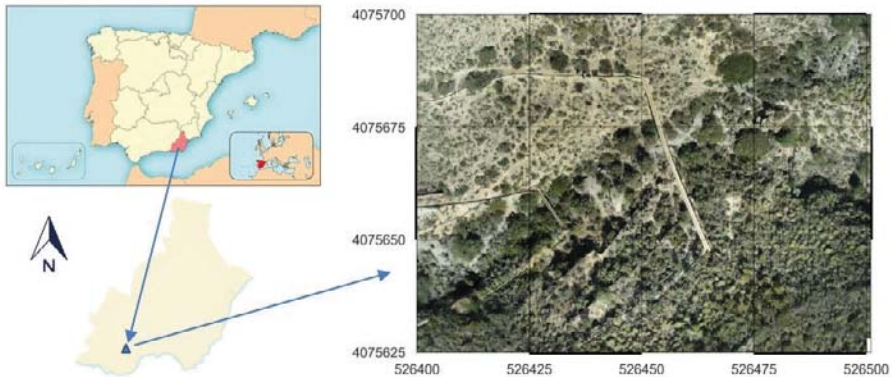


Figure 2. Location of the aqueduct under study.

## 2.2. Historical information

Although the aqueducts documented by Gil Albarracín have been assigned a Roman origin, this dating is controversial, or at least doubtful, as it is based solely on the chronology of the surrounding sites. The construction characteristics, such as concreted masonry, the presence of mechinales (drainage elements) and stucco cladding, are more typical of the Islamic Middle Ages. However, it is plausible that the aqueduct existed during Roman times and underwent repairs or expansion at later periods [37]. The irrigation infrastructure has been extensively described and studied from historical and construction perspectives [36-39]. Alternatively, some historians propose an 18th-century construction date for the aqueduct [38]. The aqueduct can be regarded as one of the most valuable elements of popular civil engineering in the region, despite its need for improved conservation. Figure 3 shows the current state of the aqueduct.



Figure 3. Current conservation state of the aqueduct.

Recently, on 23 June 2022, the Regional Ministry of Culture and Historical Heritage initiated the procedure for inscribing the aqueduct in the Catálogo General del Patrimonio Histórico Andaluz (CGPHA) as a heritage asset of cultural interest (Bien de Interés Cultural, BIC), with the typology of Monument, granting it the highest degree of protection.

## 2.3. Structural description

Above the bed of a tributary of the Carcauz wadi, one can catch a glimpse of the aqueduct arcade popularly known as the Aqueduct of the Twenty Eyes which stretches over a length of 42 m and reaches a maximum height of 9.50 m above the tributary bed. This monument is strategically positioned in a narrowing of the ravine, effectively maintaining the water level at approximately 370.8 m above sea level. The aqueduct derives its name from the 20 arches comprising its elevation. The following components of the aqueduct can be distinguished:

The base and foundations: these consist of the rocky outcrops of limestone of the ravine.

The elevation or arcade: this features three levels and twenty vaults formed by semicircular arches.

The arch on the first level, positioned at the midpoint of the structure, facilitates the passage of water of the stream through the vertical wall of the aqueduct. It stands at approximately 1.70 m from the ground to the keystone, with a span of 2.30 m. A wall is built on top of it, which is 1.12 m high above the lowest arch. Above the aforementioned first level, which rests on the limestone walls of the riverbed, a second level is defined by seven rectangular-section piers, ranging in dimension from 1.75 to 1.96 m in length and 0.80 to 1.0 m in width. These piers support eight arches of similar height. Notably, the central arch was modified by adding another arch at mid-height, approximately 1.0 m above the wall, to reinforce the structure. The third level consists of nine rectangular-section piers, measuring about 60 cm in length and 0.80 to 1.0 m in width, supporting 10 arches and their accompanying walls until they merge with the limestone walls of the ravine. These arches vary in height from 1.05 to 1.35 m and in span from 2.17 to 2.58 m, with the northernmost arch being the smallest. It seems likely that these arches were reconstructed at some point in the past, either due to damage from the passage of time or erosion caused by seismic tremors. At the crown of the aqueduct lies the water channel, with a base width ranging from 30 to 40 cm and a height of approximately 34 cm, contrasting with the 60 cm width of the irrigation channel before it enters the arcade. Notably, sediment has settled on the channel's bottom, suggesting potential modifications to the channel at a later date. The channel walls are constructed of masonry with lime mortar and are approximately 25 cm thick at the edges [40].

## **2.4. Photogrammetric survey of the aqueduct's current state**

### *2.4.1. Topographic survey for subsequent geo-referencing of photogrammetric outputs*

A traditional topographic survey was conducted using a Global Navigation Satellite System (GNSS) to accurately geo-reference the photogrammetric project and evaluate the obtained results. The survey resulted in a total of 14 targets distributed across the study area, as depicted in Figure 4c. These targets, shown in Figure 4a, were A3 format (420 mm x 297 mm) and divided into four quadrants, with two quadrants coloured orange and two black. The 3D coordinates of these targets were measured using a GNSS receiver operating in Real Time Kinematic (RTK) mode and receiving differential corrections from a base station located at the north end of the aqueduct, as illustrated in Figure 4b. Prior to this, the base station was statically positioned, and its coordinates were determined using differential corrections from the Calar Alto Station of the RAP Network (Andalusian Positioning Network) for a duration of 10 minutes. This network offers high-precision positioning across the entire Andalusian territory through free services of differential corrections and Receiver Independent Exchange Format (RINEX) files. In RTK mode, both the GNSS base and receiver receive readings from different satellite constellations, maintaining a constant data link between them in real-time, differing from the kinematic post-processing (PPK) mode.

The GNSS receiver and base station used were Emlid Reach RS2 systems. For RTK mode measurements, this multi-band geodetic receiver provides a manufacturer-stated accuracy of  $\pm 7$  mm +1 ppm for horizontal RMS and  $\pm 14$  mm +1 ppm for vertical RMS. Considering the distance between the base station and the study area was approximately 50 m, the horizontal and vertical errors are estimated to be around 7 mm and 14 mm, respectively.

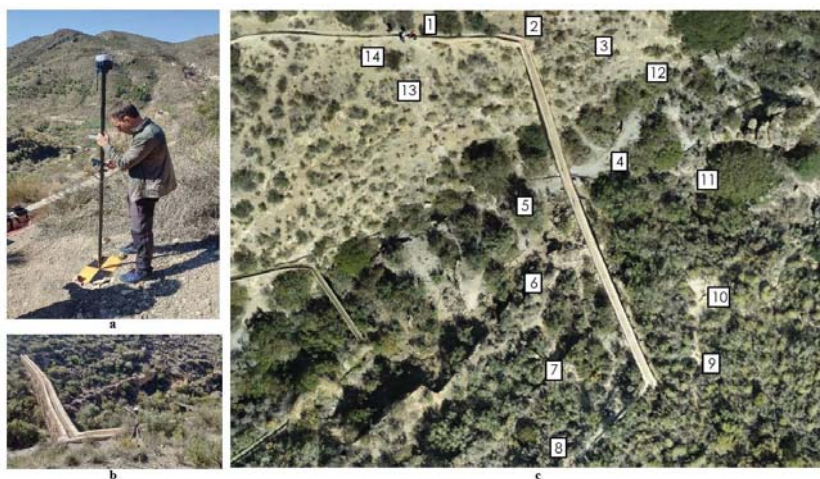


Figure 4. (a) Targets used in this study. (b) GNSS base. (c) Distribution of targets across the study area.

#### 2.4.2. Image acquisition

The images used in this project were captured using a four-rotor DJI Phantom 4 RTK UAV drone. This UAV is equipped with both GLONASS and GPS navigation systems. Additionally, it features front, rear and bottom vision systems that enable obstacle avoidance within a range of 0.2 to 7 m, as well as surface detection under defined patterns and adequate illumination. The Phantom 4 RGB camera has a 20-megapixel (5472 x 3648) 1-inch sensor, which can be manually adjusted from F2.8 to F11. The lens offers an 84° field of view and a fixed focal length of 8.8 mm.

The photogrammetric flight was autonomously planned and executed using the DJI GS RTK app. This application enables the implementation of double-grid 3D photogrammetric flights, ensuring that images of the subject are captured from various angles and inclinations. Figure 5 illustrates the trajectory followed by the drone during the photogrammetric flight. The flight, which included a total of 315 photos, was scheduled to take place at a height of 40 m from the take-off point, positioned on the north side of the aqueduct. This configuration yielded an equivalent Ground Sample Distance (GSD) of 1.22 cm/pixel. In order to enhance the precision of the photogrammetric project, the aircraft was configured to capture oblique images at a 45-degree angle as well as zenith images. Adjustments to the shutter speed were made to minimise the blurring effect on the photos, taking into account factors such as flight altitude, UAV speed and lighting conditions during the flight. The camera was activated every two seconds, and the flight speed was regulated to achieve a longitudinal and transverse overlap of 70%.

Once the flight concluded and the photographs were downloaded, the geolocation data of the cameras was corrected to enhance accuracy. For this purpose, the UAV's RTK system allows for the preservation of satellite observation information for PPK. In this instance, RINEX data at 1-second intervals, provided by the Calar Alto Station of the Andalusian RAP Network, served as the basis for corrections. Atygeo V1.8 software was used for this procedure, as it enables the correction of photo metadata from base observation and navigation files, as well as from the drone navigation file (.obs).



Figure 5. Flight path performed by the drone.

### 2.4.3. Photogrammetric process

Once the geolocation data from the cameras had been corrected, the photogrammetric process was carried out using Agisoft Metashape Professional© version 1.8.2 software. This software conducts the photogrammetric process in multiple steps using the SfM algorithm. Initially, the software identifies and matches homologous points across all photos to align them. During this process, the focal length value of the camera (extracted from the EXIF data of the photos) serves as the starting point for estimating internal and external camera parameters, including non-linear radial distortions. This step was conducted with high accuracy settings for this study. When the program concludes, it produces a sparse point cloud that includes the geometry of the aqueduct environment, each camera's specific position, orientation and an estimated set of calibration parameters. Using the geolocation data of the photographs taken by the drone, the resulting point cloud is directly georeferenced. However, this georeferencing is of low accuracy, and the use of GCP is required to improve it. At least three control points are necessary to enhance this accuracy [41-42], increasing it by using a higher number of control points. Seven (even numbers) and seven (odd numbers) of the 14 targets that were set during fieldwork will be used as GCPs and quality check points (CPs) for the completed work, georeferencing the point cloud in the ETRS89 datum and UTM Huso 30N projection. The software reoptimizes the camera calibration model and adjusts the resulting sparse point cloud after receiving the GCP to be used. Subsequently,



any anomalous points that may have emerged in the model are manually removed to create a dense point cloud comprising 11,779,429 points, thereby densifying the sparse point cloud. A highly detailed, dense point cloud constitutes the final product.

From this dense point cloud, various products can be derived, including: the triangulated mesh of the surface, onto which the texture obtained from the photographs can be applied; the Digital Surface Model and elevation model; an orthophoto of the environment; or the XYZ coordinates in .txt format of each point comprising the dense cloud created. It should be noted that a classification of the dense point cloud was carried out, combining the internal classification algorithm implemented in the Agisoft Metashape software with manual classification of certain points, such as those belonging to the aqueduct. Three classification groups were established: terrain, vegetation and aqueduct. Subsequently, the points classified as aqueduct were exported in .las format, serving as a foundation for the generation of the HBIM.

### **2.5. 3D modelling using HBIM methodology**

The BIM of the aqueduct was conducted in Autodesk Revit 2022, one of the most widely used BIM software in the world [25]. Agisoft Metashape and Autodesk Revit 2022 can be interconnected through the use of Autodesk ReCap, an additional program necessary for the Cloud-to-BIM process.

Prior to converting the project file to .rcs format, which is a point cloud format readable by Autodesk Revit, the dense point cloud obtained through UAV photogrammetry must be imported into Autodesk ReCap in .las format, containing the point cloud classified as an aqueduct. The point cloud imported into Autodesk Revit is depicted in Figure 6.



*Figure 6. Point cloud imported into Autodesk Revit.*

The incorporated information comprises a cloud with thousands of points and their associated RGB colour, showcasing the details of the actual aqueduct, from irregularities in the morphology of the vaults of the arches to variations in the thickness of the walls or their collapse along the aqueduct's directrix.

This allows us to use the visualised point cloud as a guide and reference to establish the parametric model. To complete the modelling, it was not necessary to generate libraries of parametric objects specific to the aqueduct.

Although Revit lacks automated recognition of 3D geometry from the point cloud, it

does offer tools to generate 3D objects with commonly used geometries in today's construction industry [43]. While these tools may not be typically suitable for modelling historical heritage [44] due to their specific geometries (such as ribbed vaults, cornices and lintel ornaments), they are appropriate for the HBIM intended to be generated in this work. In recent years, significant efforts have been made to generate 3D geometries through automatic point recognition. Before proceeding with the aqueduct modelling, it is essential to define the level of detail to be achieved, which closely aligns with the research objectives and required precision level.

From a graphical standpoint, three degrees of model definition can be distinguished: Grade 1 (Coarse), Grade 2 (Medium) and Grade 3 (Fine) [45].

The aim of this paper is to create a FEM for the aqueduct's structural analysis, so reaching a 3D representation level between Grades 1 and 2 will suffice. According to the terminology established by the American Institute of Architecture, we can set the Level of Development (LOD) of our BIM model between levels LOD200 and LOD300. This choice is based on simulating the aqueduct using a structural wall with a constant thickness of 0.90 m, leaning towards safety for the ensuing structural analysis.

Once the structural wall has been created, referencing the plan layout of the aqueduct, we proceed to open the aqueduct's eyes using the empty and cutting shapes tool to subtract the 'eyes of the aqueduct' from the main modelled volume. This ensures seamless interoperability between the parametric objects of the BIM model and their transformation into finite element shells for use in the structural calculation software.

## **2.6. Validation of the fit between point cloud and HBIM**

To validate each parametric object created for the HBIM, it is essential to measure the distances between the point cloud of the photogrammetric model and the mesh of the parametric object. For this validation process, the Autodesk Revit model was exported in .obj format, and together with the .txt file containing the point cloud of the aqueduct obtained from Agisoft Metashape, imported into the CloudCompare software [46]. Using the "Cloud to Mesh Distance" command in CloudCompare, the distance between both elements can be calculated. Since there is no common criterion among existing scientific literature for HBIM validation [47], the following criteria, as per Martínez-Carricondo et al. [48], were established in this research:

- The mean distance between points should be close to 0 m (between -0.10 m and 0.10 m).
- The standard deviation of the distance between points should be less than 0.10 m.

## **2.7. From building information modelling (BIM) to Finite Element Modelling (FEM)**

FEM is a numerical approximation method derived from the Matrix Method, transitioning from a 'discrete' to a 'continuous' mode. The accuracy of the FEM hinges on the size and shape of the elements into which the part is discretised. Moreover, the inclusion of 2D and 3D elements provides significantly higher accuracy in result derivation compared to a model solely comprised of 1D bars.

FEM is mathematically more complex than other linear methods, such as the matrix

method. However, it offers greater precision and, notably, enhanced capacity to model structures beyond the scope of bar elements. While its mathematical manipulation may be cumbersome, we are fortunate to have numerous software applications capable of swiftly generating and solving the numerical equations inherent in this method. This allows designers to discern the true behaviour of their structures, reducing their workload to inputting initial data and analysing results. For this project, the SAP2000 software developed by Computers & Structures, INC. was used.

The objective of this research was to develop a FEM to enable the study of the structural behaviour of the Twenty Eyes Aqueduct.

To achieve this, it was imperative to convert the HBIM into a 3D model with geometric elements compatible with SAP2000. This software was selected because it allows the import of solid 3D elements or 2D shells geometry, followed by discretisation or meshing. Given the linear nature of the structure in this project, it was decided to model it using 2D shell-type elements. The primary advantages of this approach include minimising structural calculation times and simplifying stress analysis.

Starting from a 3D HBIM to generate the finite element calculation model saves considerable time in the development phase of the FEM. Additionally, it leverages the advantage of having greater detail compared to the typical simplified models often adopted for such purposes [35]. The process to generate the FEM involved several steps. First, the BIM model of the aqueduct was exported to .dwg format for further processing in AutoCAD 3D. The resulting product consisted of polyface meshes defining the entire geometry. The polyface meshes were then subdivided into smaller secondary meshes, both horizontally and vertically, each bounded by four edges. To achieve the desired final discretisation size for accurate structural analysis, the aqueduct was manually divided into 10 sections.

Finally, these secondary meshes were decomposed into 'Cara 3D' elements, facilitating their import into the SAP2000 software as 'shell' elements. Once the 3D face elements were imported into SAP2000, the FEM depicted in Figure 7 was obtained, consisting of 4,170 area or shell elements. To control the model's complexity and ensure efficient computational performance, the average mesh size was set to less than 0.50 m, guaranteeing high-quality results.

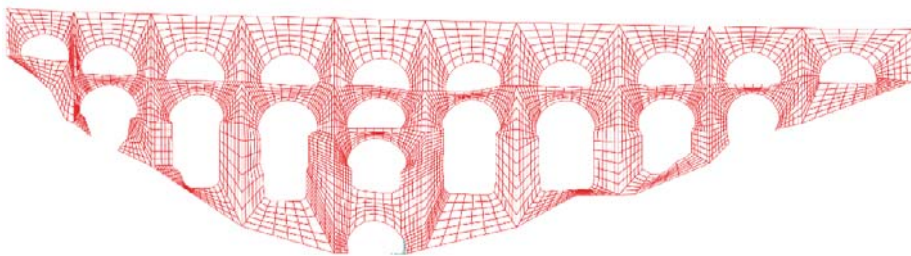


Figure 7. Model imported into SAP2000.

Once the geometry of the model is available in SAP2000, it is essential to input all the required initial information for the software to perform the calculations.

This includes defining the mechanical properties of the stone-mortar assembly constituting the aqueduct, specifying the external loads acting on the structure and establishing the boundary conditions affecting its structural behaviour, particularly its support on the ground.

### 2.7.1. Characteristics of the materials

The masonry construction of the Twenty Eyes Aqueduct consists of a series of stone pieces assembled and bonded with mortar. The composition of the masonry primarily comprises the characteristics of the stone pieces and mortar, the latter sometimes being absent [49]. For this study, no destructive characterisation tests were conducted on the aqueduct structure. Instead, a visual and geological analysis of the area was performed. Considering the limestone nature of the rock found in the ravine of the Carcauz wadi, the properties of the stone material constituting the aqueduct were estimated. The mechanical properties of the masonry were determined based on its elastic modulus, Poisson's coefficient and the specific weight of the material.

According to J. A. Martín Caro [49], the specific weight of limestone ranges between 20 and 26 kN/m<sup>3</sup>. However, the specific weight of the masonry composite material is determined by the weighted average of the components based on their respective proportions in volume. Considering that in stone masonry constructions, the volume of mortar is significantly lower than that of stone, we can estimate the specific weight of the composite material to be 20 kN/m<sup>3</sup>, adopting a conservative value. The modulus of elasticity ( $E_b$ ) of limestone falls between 17,000 and 76,000 N/mm<sup>2</sup>, with a Poisson's ratio ranging from 0.15 to 0.20. For lime mortar, a modulus of elasticity ( $E_m$ ) is considered to be between 400 and 2000 N/mm<sup>2</sup>, with a Poisson's ratio of 0.2. While mortar, being less rigid, primarily contributes to the masonry's deformability, understanding the modulus of elasticity of both components is important, as it influences the composite material's behaviour. Equation 1 provides an indicative value for the longitudinal deformation modulus (E) of the part-mortar assembly.

$$E = 0,50 * E_b = 0,5 * 17000 \text{ N/mm}^2 = 8500 \text{ N/mm}^2 \quad (1)$$

A Poisson's ratio of 0.15 will be adopted for the entire masonry structure.

### 2.7.2. Structural loads

Below are descriptions of all the actions acting on the aqueduct, along with justifications for the values adopted and an analysis of the suitability of the loads taken into account:

- Permanent loads: the dead weight of all masonry elements was calculated based on their geometrical characteristics, considering a specific weight of the masonry of 20 kN/m<sup>3</sup>.
- Variable loads: treating the aqueduct as a vertical wall with several openings subjected to wind action, wind pressure was calculated following Eurocode 1 (UNE 1991-1-4:2005), resulting in a value of wind pressure on the external surface:

$$w_e \approx 1,00 \text{ kN/m}^2$$

This action was applied to both facades of the aqueduct, acting in one direction for the 'Wind +' scenario and in the opposite direction for the 'Wind -' scenario.

- Accidental loads: Seismic action was considered by conducting a modal-spectral analysis with SAP2000, following the recommendations of the Seismic Resistant Standard NCSE-02.

### 2.7.3. Combination of loads

The load hypotheses considered are formed by combining the calculation values of the actions whose effects may be simultaneous (concomitant actions), according to the general criteria prescribed in the Technical Building Code of the Spanish Ministry of Housing, for both Ultimate Limit States and Serviceability Limit States.

The following table shows the combinations of load assumptions for the Ultimate Limit States of Stability and Strength of the aqueduct (ELU) and the Serviceability Limit States of Deformation (ELS), indicating the coefficients of action magnification. For stability checks, the global loads provided by the software for each individual scenario were used.

### 2.7.4. Boundary conditions

The aqueduct rests directly on the rocky outcrops visible in the riverbed, as determined by the field visit and visual inspection of the aqueduct foundations. Additionally, a continuous footing, also composed of masonry, could have been laid at those valley locations where there was a superficial layer of fill.

Table 1. FEM calculation combinations

Combination	Simple hypotheses					Analysis
	Dead-weight	Wind X+	Wind X-	Seism X	Seism Y	
1-ELU	1,35	1,50	-	-	-	Resistance
2-ELS	1,00	1,00	-	-	-	Deformations
3-ELU	1,35	-	1,50	-	-	Resistance
4-ELS	1,00	-	1,00	-	-	Deformations
5-ELU	1,00	-	-	1,00	0,30	Resistance and Deformations
6-ELU	1,00	-	-	0,30	1,00	Resistance and Deformations

*ELU = Ultimate Limit States of Stability and Resistance*

*ELS = Deformation Service Limit States*

Based on observations, the foundation of the aqueduct base appears to be between that of a simple support and an embedment. Given that a significant portion of the aqueduct wall is inserted into the limestone rock massif, it makes sense that contour conditions would be used throughout the entire lower edge of the aqueduct model to simulate an embedded support in order to reach the level of analysis required for this investigation. In order to fulfil the purpose of the present work, it was sufficient to analyse the model described with the boundary conditions of embedment at the base of the aqueduct.

### 3. Results

#### 3.1. Results of the photogrammetric process

In the established workflow, the first results we obtained were those of the point cloud of the aqueduct area. The accuracy of the photogrammetric project is shown in Table 2, where the error obtained in each CP is displayed.

Table 2. Errors obtained in the Check Points (Agisoft Metashape Report)

Check Point	Error in X (cm)	Error in Y (cm)	Error in Z (cm)	Total error (cm)	Image Error (pix)
2	1.66399	-3.1027	0.0259657	3.52084	0.311 (188)
4	0.341269	-3.91809	1.57669	4.2372	0.257 (235)
6	-1.25744	2.02388	-0.218058	2.39265	0.263 (213)
8	-1.44521	1.09357	-2.4372	3.03718	0.292 (219)
10	2.0657	1.23115	-2.28027	3.31397	0.297 (224)
12	0.482149	-1.82293	-1.0632	2.16471	0.301 (207)
14	1.22377	-4.85691	1.01957	5.11143	0.277 (169)
Total	1.3391	2.89577	1.50445	3.52733	0.286

#### 3.2. Results of the HBIM

In the established workflow, after classifying the points of the cloud in Agisoft Metashape and exporting the points classified as 'aqueduct', a point cloud with a total of 284,779 points was obtained and imported into the Autodesk Revit software for the creation of the HBIM.

According to the methodology described in the previous section, the geometric characteristics of the aqueduct were modelled using the point cloud as a guide.

Figure 8 shows the model created in Autodesk Revit 2022 and its overlay with the point cloud.

#### 3.3. Results of the HBIM validation

Once the HBIM was created, it was necessary to validate the accuracy of the adjustment made in relation to the point cloud. Figure 9 shows the results of the comparative analysis between both elements carried out using the CloudCompare software. The mean of the differences detected between the HBIM object created and the photogrammetric model (point cloud) is 0.022 m, with these differences centred in the majority of points within the range of -0.10 m to 0.10 m. The standard deviation obtained is 0.08 m. The results are represented on a colour scale that highlights the differences,

with points showing the worst correspondence in red and those with the best representation in the generated model in green.

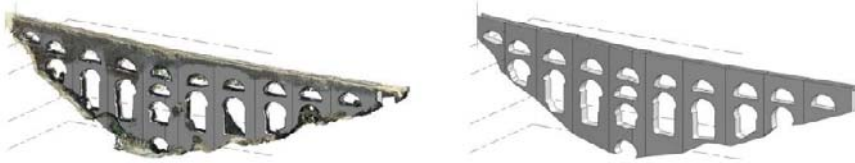


Figure 8. Model created in Autodesk Revit 2022 overlaid with the point cloud.

### 3.4. Results of the structural calculation

The last step in the workflow described in section 2 is the generation and analysis of the FEM. This analysis was carried out by a computer with Intel(R) Core (TM) i7-8700K CPU 3.70GHz and 16 Gb RAM in a time of eight seconds. The model is composed of 4,627 points and 4,170 area or shell elements. After analysing the stability of the assembly in the event of overturning and sliding, the tensile and resistant behaviour of the masonry and the deformations produced in the vertical wall of the aqueduct, the following results were obtained. The stability of the construction was determined by calculating the coefficients of safety against overturning (CSV) and sliding (CSD), assuming that the assembly behaves as a rigid solid.

The following reactions were obtained from the calculation model in SAP2000:

- The overall Z-reaction due to the self-weight of the aqueduct is 2979.4 kN.
- The overall reaction in the X-direction (perpendicular to the aqueduct wall) due to the wind effect is 163.3 kN.
- The overall reaction in the X-direction (perpendicular to the aqueduct wall) due to the effect of seismic activity is 447.9 kN.
- An average height of  $h = 3.40$  m was determined for each section of the aqueduct, which is the position at which the forces resulting from wind and earthquake are applied for the purposes of the stability checks. A coefficient of friction between the ground and the structure of  $\mu = 0.55$  was estimated. Furthermore, the aqueduct wall has an average thickness of 0.90 m.

A CSV and a CSD value were found for the most unfavourable stability combination involving wind action:

$$CSV = \frac{\text{Stabilising momentums}}{\text{Destabilising momentums}} = \frac{2979,4 \text{ kN} * \frac{1}{2} * 0,90 \text{ m}}{163,3 \text{ kN} * 3,40 \text{ m}} = 2,41$$

$$CSD = \frac{\text{Stabilising strengths}}{\text{Destabilising strengths}} = \frac{2979,4 \text{ kN} * 0,55}{163,3 \text{ kN}} = 10,03$$

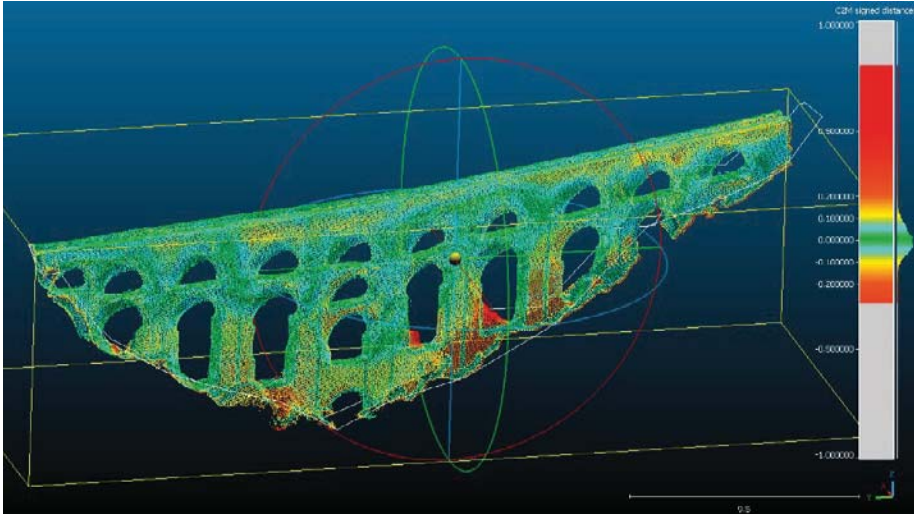


Figure 9. Validation of the HBIM of the aqueduct in CloudCompare.

For the worst-case stability combination involving earthquake action, a CSV and a CSD value were obtained:

$$CSV = \frac{\text{Stabilising momentums}}{\text{Destabilising momentums}} = \frac{2979,4 \text{ kN} * \frac{1}{2} * 0,90 \text{ m}}{447,9 \text{ kN} * 3,40 \text{ m}} = 0,88$$

$$CSD = \frac{\text{Stabilising strengths}}{\text{Destabilising strengths}} = \frac{2979,4 \text{ kN} * 0,55}{447,9 \text{ kN}} = 3,66$$

To analyse the structural stress and resistance of the aqueduct, without being exhaustive, the stresses induced in the aqueduct walls were extracted from the SAP2000 model according to the combinations indicated in section 2.7.3.

For the simple deadweight hypothesis, the following horizontal (Figure 10) and vertical (Figure 11) axial stresses were obtained:

In Figure 11, a maximum compression value of -315.8 kN/m is observed, with practically zero tensile stresses.

The horizontal actions of wind and earthquake are mainly characterised by bending and shear forces at the base of the aqueduct wall. For the combinations that consider the action of wind (1-ELU and 3-ELU), the forces obtained in the shell elements in which the aqueduct has been discretised are those shown in Figure 12 (moments) and Figure 13 (shear). For the combinations that contemplate the action of the seismic activity (5-ELU and 6-ELU), the stresses obtained are those shown in Figure 14 (moments) and Figure 15 (shear).

In Figure 10, a maximum compression value of -65.6 kN/m and a maximum tensile value of 79.7 kN/m can be observed.

In Figure 12, a maximum bending moment at the base of the aqueduct of 37.1 kN\*m/m is observed.

In Figure 13, a maximum shear value of 15.6 kN/m is observed.



In Figure 14, a maximum bending moment at the base of the aqueduct of 133.2 kN\*m/m is observed.

In Figure 15, a maximum shear value of 47.8 kN/m is observed.

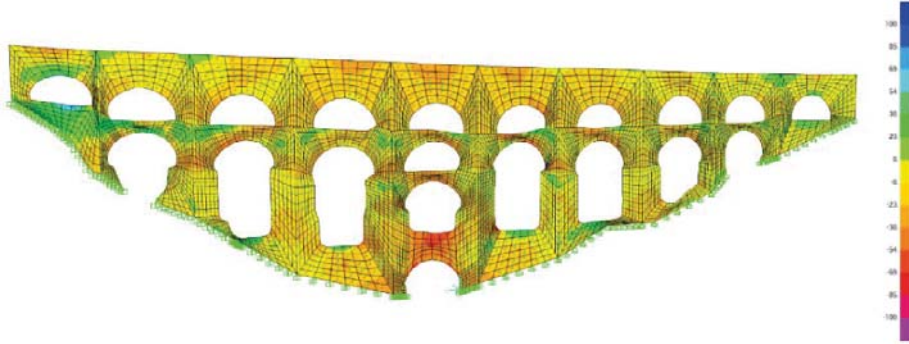


Figure 10. Horizontal axial stresses due to deadweight.

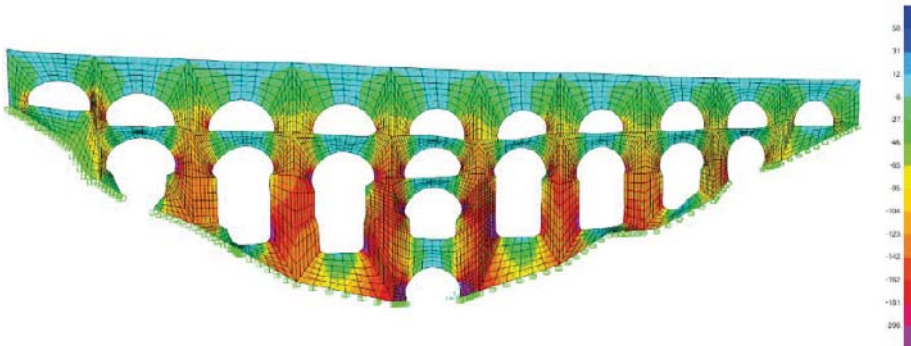


Figure 11. Vertical axial stresses due to deadweight.

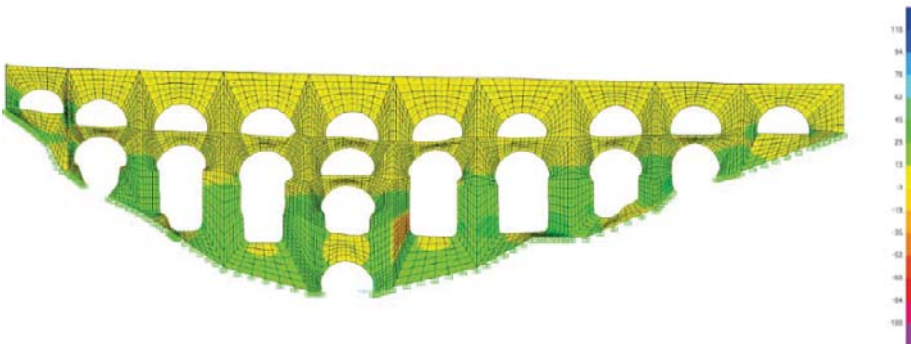


Figure 12. Bending stresses for the 1-ELU combination.

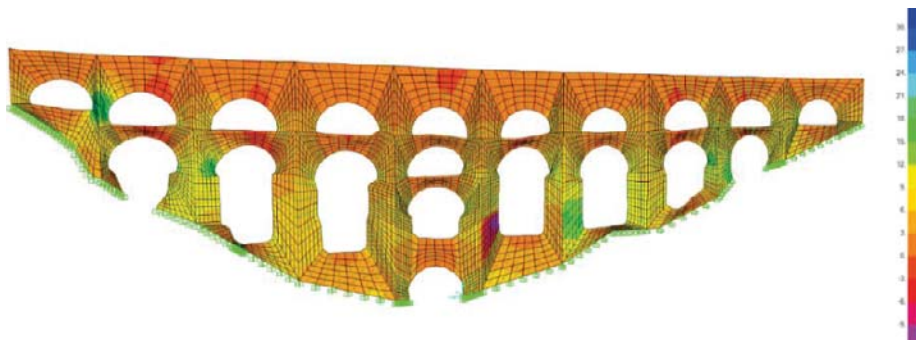


Figure 13. Shear stresses ( $V_{max}$ ) for the 1-ELU combination.

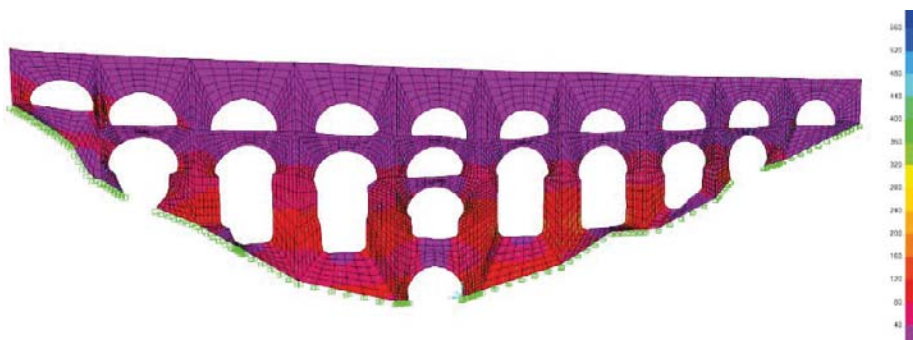


Figure 14. Bending stresses for the 5-ELU combination.

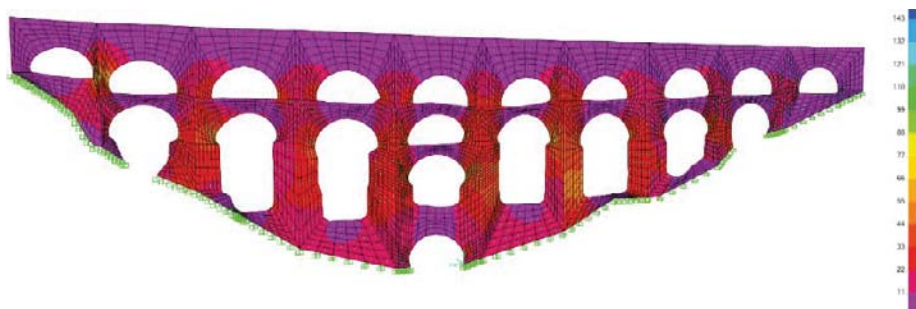


Figure 15. Shear stresses ( $V_{max}$ ) for the 5-ELU combination.

Finally, the resulting deformations in the structure due to the combinations considering the action of wind in the Serviceability Limit State (2-ELS and 4-ELS) and earthquakes (5-ELU and 6-ELU) are presented.

Figure 16 shows a maximum aqueduct crown displacement of 1.6 mm.

Figure 17 shows a maximum aqueduct crown displacement of 6.2 mm.

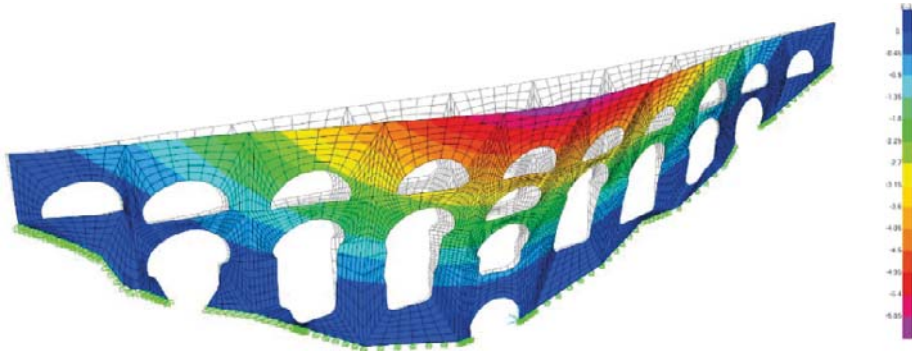


Figure 16. Horizontal offsets for the 4-ELS combination. Scale increased by x500.

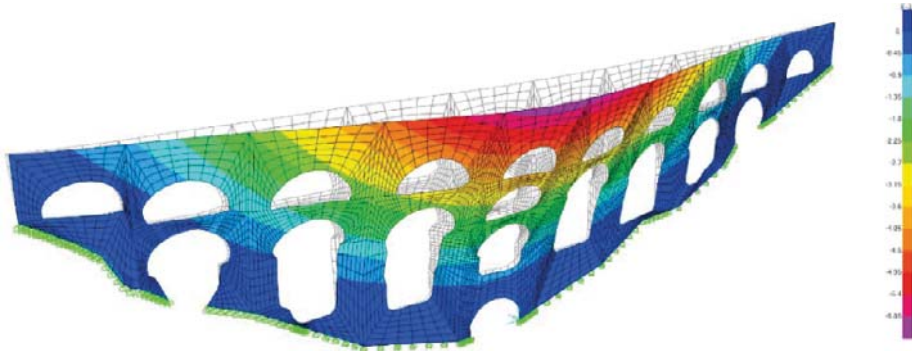


Figure 17. Horizontal offsets for the 5-ELU combination. Scale increased by x500.

#### 4. Discussion

The maintenance of antique infrastructures, particularly those lacking original project documentation, presents a significant challenge, as previously noted. Regardless of the infrastructure type, understanding its structure is crucial for effective maintenance and to ensure operational functionality throughout its lifecycle, as seen in various environments such as ports and maritime settings [50]. In cultural heritage elements like the one examined in this study, analysing structural stability is paramount to prevent infrastructure collapse. The reverse engineering process conducted through UAV photogrammetry or laser scanning has been applied in numerous building restoration projects [51-53]. However, this study added complexity by requiring precise modelling of the arches' eyes, necessitating the use of oblique images and flights in various directions and at different altitudes.

##### 4.1. Accuracy of the photogrammetric project

The values obtained in the photogrammetric project align with several practical applications examined by Clapuyt et al. [54], who compared 10 cases of 3D topographic

reconstructions based on the SfM algorithm under conditions similar to those at the aqueduct site. Additionally, other studies which focused on historical heritage have tolerated errors of up to 15 cm [30, 48], with accuracy typically measured within a cm.

In this research, the total error in the georeferenced model is 3.53 cm and is considered sufficiently accurate for the type of analysis conducted, even comparable to results achievable with TLS analysis [17].

#### **4.2. Use of oblique images**

The enhancement of accuracy and detail in point clouds acquired through UAV photogrammetry with oblique photography has been demonstrated in numerous studies [55, 56]. In this study, the photogrammetric project used photographs captured at a close distance to the object, with camera tilt angles of 45° and 90°, eliminating the need for ground photographs. These conditions resemble the approach in a study of the Piedmont monastery in Italy [55], where high accuracy was also achieved. Undoubtedly, the use of photographs taken at varying angles proved beneficial in obtaining a more precise point cloud of the aqueduct.

#### **4.3. Accuracy of the HBIM**

According to the specific scientific literature, there are no established accuracy limit values for HBIMs created through a point cloud. The level of accuracy should be selected based on the type of intervention or analysis to be conducted, aiming to generate a model that is easy to manage and interpret [2]. In this study, limits were set to ensure the accurate structural interpretation of the aqueduct model and to facilitate the transformation from the HBIM to the FEM without significant simplification. Most observed differences do not exceed 10 cm, primarily resulting from default assumptions, such as considering smaller structural sections than those actually present, ensuring a conservative approach in analysing the structural behaviour. Additionally, factors such as landslides and material accumulations in the aqueduct's eyes, while not structurally significant, contribute to minor adjustment differences in some areas.

#### **4.4. Accuracy of the FEM**

The accurate representation of the aqueduct's geometry in the HBIM poses challenges in creating an exportable object readable by SAP2000 calculation software. Therefore, certain aspects, such as the variability in wall thickness and observed overhangs, were simplified to facilitate information exchange between software platforms. These simplifications, while necessary for interoperability, were implemented with minimal impact on the analysis results, prioritising safety in structural analysis and maintaining high geometric accuracy in the model. Interoperability issues encountered between Autodesk Revit and SAP2000 led to the development of the FEM using Autodesk AutoCAD 3D software, an area of ongoing research to enable automated transitions. The average mesh size in the FEM was deemed adequate for this study, with the maximum distance between nodes on the same edge of shell elements not exceeding 50 cm.

Finer meshing may not significantly alter conclusions [57-58] but would increase computation times, so larger elements were maintained for efficiency.

#### 4.5. Structural behaviour of the aqueduct

Based on the assessment of the aqueduct's stability against external forces, it appears that the structure is adequately resistant to wind and gravitational forces, mitigating both overturning and sliding risks. However, its stability against overturning would be compromised in the event of a seismic disturbance. According to the Ministry of Housing's CTE standards, the CSV coefficient should exceed 2, while the CSD coefficient should surpass 1.5. However, the obtained CSV value for seismic actions is 0.88, falling short of the unit and significantly below the CTE requirement. Consequently, further investigation into potential reinforcement strategies for the monument is needed to ensure its stability under various scenarios specified by existing regulations.

Regarding the distribution of stresses induced in the aqueduct due to its own weight, the model's outcomes are consistent. Horizontal compressions are evident in the arch vaults, while vertical compressions are observed in the piers, with their magnitude increasing towards the base. This aligns with the typical structural behaviour expected from such constructions. Regarding the maximum axial forces resulting from the aqueduct's weight, it is noteworthy that the compressive stresses observed in the masonry are considerably lower than the characteristic compressive strength of both limestone (ranging between 25 and 130 N/mm<sup>2</sup>) and lime mortar (between 0.5 and 2 N/mm<sup>2</sup>). Similarly, tensile stresses are also notably lower than the tensile strength of the stone, which various sources estimate at around 5% of the characteristic compressive strength [49].

$$\sigma_{compress} = \frac{N}{A} = \frac{315800 \text{ N}}{1000 \text{ mm} * 900 \text{ mm}} = 0,35 \text{ N/mm}^2$$

$$\sigma_{tensile} = \frac{N}{A} = \frac{79700 \text{ N}}{1000 \text{ mm} * 900 \text{ mm}} = 0,089 \text{ N/mm}^2$$

Where:

$\sigma$ : Stress (N/mm<sup>2</sup>)

N: Axil stress (N)

A: Section area (mm<sup>2</sup>)

However, to derive accurate conclusions regarding the resistance behaviour of the aqueduct, it is essential to analyse the design combinations in greater detail, considering the effects of wind and earthquake. An approximation of the maximum compressive stresses to be endured by the critical section of the aqueduct can be made by applying the Navier formula for sections subjected to bending and axial force:

$$\sigma = \frac{N}{A} \pm \frac{M * y}{I}$$

Where:

$\sigma$ : Stress (N/mm<sup>2</sup>)

N: Axil stress (N)

A: Section area (mm<sup>2</sup>)

M: Bending moment (N\*mm)

y: Distance from the neutral axis to the most compressed fibre (mm)

I: Inertia of the section (mm<sup>4</sup>)

In the seismic scenario, which results in the maximum bending moment at the base

of the aqueduct, there would be an increase in compressive stresses within the section due to the magnitude of the bending moment:

$$\sigma = \frac{M * y}{I} = \frac{133,2 \text{ kN} * \text{m} * 10^6 * 450 \text{ mm}}{\frac{1}{12} * 1000 * 900^3} = 0,99 \text{ N/mm}^2$$

If we add the compressive stress generated by the bending moment in the seismic combination to the compressive stresses arising from the axial forces on the section, the resulting stresses will still be significantly below the characteristic compressive strength of the masonry [60, 61].

Finally, it should be noted that the horizontal deformations observed in the model due to the effects of wind and earthquake remain within the limit values for total collapse established by the CTE and other international regulations.

The total collapse ( $\delta$ ) for combinations involving wind action must not exceed 1/500 of the total height of the aqueduct. In this case, the observed elastic displacement is 1.6 mm, and the maximum height above the aqueduct bed is 9.50 m. Therefore, according to current regulations, a displacement of up to 1.9 cm would be allowed, which is significantly higher than the modelled value.

$$\delta \leq \frac{9,50 \text{ m}}{500} = 0,019 \text{ m}$$

The total collapse ( $\delta$ ) for combinations involving earthquake action must not exceed 1/100 of the total height of the aqueduct. In this case, the observed elastic displacement is 6.2 mm. Therefore, according to current standards, a displacement of up to 9.5 cm would be allowed, which is considerably higher than the modelled value.

$$\delta \leq \frac{9,50 \text{ m}}{100} = 0,095 \text{ m}$$

It is true that these displacements would be higher if non-elastic behaviour of the masonry were considered. However, the values obtained are sufficiently far from the normative limit to consider, for this level of study, acceptable behaviour in ELS of aqueduct deformations.

## 5. Conclusions

The Cloud-to-BIM-to-FEM methodology enables the generation of BIM and FEM models of architectural and engineering works with low cost, flexibility and high-quality results. This makes it an essential tool for the reconstruction, protection and conservation of our historical heritage.

The photogrammetric project carried out has shown competitive results compared to surveys conducted with TLS. The combination of zenith and oblique images has significantly improved the dense point cloud obtained from the photogrammetric process.

The process of generating the HBIM has consistently maintained the final objective of the work in mind, avoiding unjustified simplifications and resulting in a reliable representation of the aqueduct. A validation process was applied to ensure the similarity between the parametric object created in the HBIM and the dense point cloud from the photogrammetric project, ensuring a high geometric fit between the models. This

facilitates the subsequent accurate structural interpretation of the aqueduct.

The HBIM accurately reflects the geometric complexity of the aqueduct, while the FEM captures its irregularities without oversimplifying the structure. This is a significant improvement over traditional simulations, which often rely on overly simplistic models of masonry works.

Future developments will require the implementation of advanced functionalities to automate the conversion from BIM to FEM. Existing BIM-to-FEM solutions are typically applicable only to regular buildings with highly standardised layouts [33, 59, 60].

The structural analysis of the FEM successfully evaluated the instability conditions of the building in the event of an earthquake, although it exhibits satisfactory behaviour in the event of wind. With regard to the tensile behaviour of the aqueduct walls, it is evident that the maximum compressions experienced by the masonry are significantly below the characteristic resistance of the ensemble formed by the masonry pieces and the lime mortar binding them. However, further analysis considering the non-linearity of masonry behaviour will be necessary to determine whether the tensions generated in the walls could lead to unacceptable compressions or instances of rupture in certain sections.

This point paves the way for future research aimed at identifying areas where tension occurs, which must be addressed to ensure the future structural integrity of this cultural heritage asset over the years. Additionally, it sets the stage for drafting a rehabilitation project for the monument. Another intriguing avenue of exploration would involve the realistic virtual reconstruction of the aqueduct, serving as a means to disseminate the rich historical heritage found in the province of Almeria.

## References

- [1] F. Chionna, F. Argese, V. Palmieri, I. Spada, and L. Colizzi, (2015) "Integrating building information modeling and augmented reality to improve investigation of historical buildings," *Conservation Science in Cultural Heritage*, vol. 15, no. 1, 2015, doi: 10.6092/issn.1973-9494/6174.
- [2] C. Biagini, P. Capone, V. Donato, and N. Facchini (2016) "Towards the BIM implementation for historical building restoration sites," *Autom Constr*, vol. 71, pp. 74–86, doi: 10.1016/j.autcon.2016.03.003.
- [3] Q. Guo, H. Liu, F. M. Hassan, M. W. Bhatt, and A. M. Buttar (2022) "Application of UAV tilt photogrammetry in 3D modeling of ancient buildings," *International Journal of System Assurance Engineering and Management*, vol. 13, doi: 10.1007/s13198-021-01458-4.
- [4] F. Chiabrando, F. Nex, D. Piatti, and F. Rinaudo (2011) "UAV and RPV systems for photogrammetric surveys in archaeological areas: Two tests in the Piedmont region (Italy)," *J Archaeol Sci*, vol. 38, no. 3, pp. 697–710, doi: 10.1016/j.jas.2010.10.022.
- [5] T. Bakirman *et al.* (2020) "Implementation of ultra-light UAV systems for cultural heritage documentation," *J Cult Herit*, vol. 44, pp. 174–184, doi: 10.1016/j.culher.2020.01.006.
- [6] S. F. El-Hakim, J. A. Beraldin, M. Picard, and G. Godin (2004) "Detailed 3D reconstruction of large-scale heritage sites with integrated techniques," *IEEE Comput Graph Appl*, vol. 24, no. 3, pp. 21–29, doi: 10.1109/MCG.2004.1318815.
- [7] F. Galeazzi (2017) "3D recording, documentation and management of cultural heritage," *International Journal of Heritage Studies*, vol. 23, no. 7, pp. 671–

- 673, doi: 10.1080/13527258.2017.1300933.
- [8] C. Liu, Y. Cao, C. Yang, Y. Zhou, and M. Ai (2020) "Pattern identification and analysis for the traditional village using low altitude UAV-borne remote sensing: multifeatured geospatial data to support rural landscape investigation, documentation and management," *J Cult Herit*, vol. 44, pp. 185–195, doi: 10.1016/j.culher.2019.12.013.
- [9] F. Remondino (2011) "Heritage recording and 3D modeling with photogrammetry and 3D scanning," *Remote Sens (Basel)*, vol. 3, no. 6, pp. 1104–1138, doi: 10.3390/rs3061104.
- [10] H. Rüther *et al.* (2009) "Laser scanning for conservation and research of African cultural heritage sites: the case study of Wonderwerk Cave, South Africa," *J Archaeol Sci*, vol. 36, no. 9, pp. 1847–1856, doi: 10.1016/j.jas.2009.04.012.
- [11] I. Colomina and P. Molina (2014) "Unmanned aerial systems for photogrammetry and remote sensing: A review," *ISPRS Journal of Photogrammetry and Remote Sensing*, vol. 92, pp. 79–97, doi: 10.1016/j.isprsjrs.2014.02.013.
- [12] J. Fernández-Hernandez, D. González-Aguilera, P. Rodríguez-González, and J. Mancera-Taboada (2014) "Image-Based Modelling from Unmanned Aerial Vehicle (UAV) Photogrammetry: An Effective, Low-Cost Tool for Archaeological Applications," *Archaeometry*, vol. 57, no. 1, pp. 128–145, doi: 10.1111/arc.12078.
- [13] R. Tomás, A. Riquelme, M. Cano, and A. Abellán (2016) "Structure from Motion (SfM): una técnica fotogramétrica de bajo coste para la caracterización y monitoreo de macizos rocosos.," *10º Simposio Nacional de Ingeniería Geotécnica, A Coruña, España*, vol. 1, no. 1.
- [14] Y. Furukawa and C. Hernández (2015) "Multi-view stereo: A tutorial," *Foundations and Trends in Computer Graphics and Vision*, vol. 9, no.1–2, doi: 10.1561/06000000052.
- [15] C. Hugenholtz *et al.* (2016) "Spatial accuracy of UAV-derived orthoimagery and topography: Comparing photogrammetric models processed with direct geo-referencing and ground control points," *Geomatica*, vol. 70, pp. 21–30, doi: 10.5623/cig2016-102.
- [16] M. Korumaz *et al.* (2017) "An integrated Terrestrial Laser Scanner (TLS), Deviation Analysis (DA) and Finite Element (FE) approach for health assessment of historical structures. A minaret case study," *Eng Struct*, vol. 153, pp. 224–238, doi: 10.1016/j.engstruct.2017.10.026.
- [17] P. Martínez-Carricondo, F. Agüera-Vega, and F. Carvajal-Ramírez (2020) "Use of UAV-photogrammetry for Quasi-vertical wall surveying," *Remote Sens (Basel)*, vol. 12, no. 14, p. 2221, doi: 10.3390/rs12142221.
- [18] J. Fernández-Lozano and G. Gutiérrez-Alonso (2017) "The Alejico Carboniferous Forest: a 3D-Terrestrial and UAV-Assisted Photogrammetric Model for Geologic Heritage Preservation," *Geoheritage*, vol. 9, pp. 163–173, doi: 10.1007/s12371-016-0193-0.
- [19] C. Achille *et al.* (2015) "UAV-based photogrammetry and integrated technologies for architectural applications—methodological strategies for the after-quake survey of vertical structures in Mantua (Italy)," *Sensors (Switzerland)*, vol. 15, pp. 15520–15539, doi: 10.3390/s150715520.
- [20] Y. Tan, S. Li, H. Liu, P. Chen, and Z. Zhou (2021) "Automatic inspection data collection of building surface based on BIM and UAV," *Autom Constr*, vol. 131, doi: 10.1016/j.autcon.2021.103881.
- [21] Y. Lin, M. Jiang, Y. Yao, L. Zhang, and J. Lin (2015) "Use of UAV oblique imaging for the detection of individual trees in residential environments," *Urban*



- For Urban Green*, doi: 10.1016/j.ufug.2015.03.003.
- [22] A. Vetrivel, M. Gerke, N. Kerle, and G. Vosselman (2015) "Identification of damage in buildings based on gaps in 3D point clouds from very high resolution oblique airborne images," *ISPRS Journal of Photogrammetry and Remote Sensing*, vol. 105, pp. 61–78, doi: 10.1016/j.isprsjprs.2015.03.016.
- [23] S. Azhar (2011) "Building information modeling (BIM): Trends, benefits, risks, and challenges for the AEC industry," *Leadership and Management in Engineering*, vol. 11, no. 3, doi: 10.1061/(ASCE)LM.1943-5630.0000127.
- [24] R. Charef, H. Alaka, and S. Emmitt (2018) "Beyond the third dimension of BIM: A systematic review of literature and assessment of professional views," *Journal of Building Engineering*, vol. 19, doi: 10.1016/j.jobe.2018.04.028.
- [25] K. Ullah, I. Lill, and E. Witt (2019) "An overview of BIM adoption in the construction industry: Benefits and barriers," in *10th Nordic Conference on Construction Economics and Organization*, Emerald Publishing Limited, pp. 297–303. doi: 10.1108/S2516-285320190000002052.
- [26] S. Logothetis, A. Delinasiou, and E. Stylianidis (2015) "Building information modelling for cultural heritage: A review," in *ISPRS Annals of the Photogrammetry, Remote Sensing and Spatial Information Sciences*, doi: 10.5194/isprsannals-II-5-W3-177-2015.
- [27] D. P. Pocobelli, J. Boehm, P. Bryan, J. Still, and J. Grau-Bové (2018) "BIM for heritage science: a review," *Herit Sci*, vol. 6, no. 1, doi: 10.1186/s40494-018-0191-4.
- [28] M. Murphy, E. MCGovern, and S. Pavia (2009) "Historic building information modelling (HBIM)," *Structural Survey*, vol. 27, no. 4, doi: 10.1108/02630800910985108.
- [29] M. G. Angelini, V. Baiocchi, D. Costantino, and F. Garzia (2017) "Scan to BIM for 3D reconstruction of the papal basilica of saint Francis in Assisi In Italy," *International Archives of the Photogrammetry, Remote Sensing and Spatial Information Sciences - ISPRS Archives*, vol. 42, no. 5W1, pp. 47–54, doi: 10.5194/isprs-Archives-XLII-5-W1-47-2017.
- [30] P. Martínez-Carricondo, F. Carvajal-Ramírez, L. Yero-Paneque, and F. Agüera-Vega (2021) "Combination of HBIM and UAV photogrammetry for modelling and documentation of forgotten heritage. Case study: Isabel II dam in Níjar (Almería, Spain)," *Herit Sci*, vol. 9, no. 1, pp. 1–15, Dec. 2021, doi: 10.1186/S40494-021-00571-8/FIGURES/16.
- [31] C. Rodríguez-Moreno, J. F. Reinoso-Gordo, E. Rivas-Lpez, A. Gmez-Blanco, F. J. Ariza-Lpez, and I. Ariza-Lpez (2016) "From point cloud to BIM: an integrated workflow for documentation, research and modelling of architectural heritage," *Survey Review*, vol. 50, no. 360, pp. 212–231, doi: 10.1080/00396265.2016.1259719.
- [32] Y. Tan, G. Li, R. Cai, J. Ma, and M. Wang (2022) "Mapping and modelling defect data from UAV captured images to BIM for building external wall inspection," *Autom Constr*, vol. 139, doi: 10.1016/j.autcon.2022.104284.
- [33] L. Barazzetti, F. Banfi, R. Brumana, G. Gusmeroli, M. Previtali, and G. Schiantarelli (2015) "Cloud-to-BIM-to-FEM: Structural simulation with accurate historic BIM from laser scans," *Simul Model Pract Theory*, vol. 57, pp. 71–87, doi: 10.1016/j.simpat.2015.06.004.
- [34] M. Bassier, G. Hadjidemetriou, M. Vergauwen, N. Van Roy, and E. Verstrynge (2016) "Implementation of Scan-to-BIM and FEM for the Documentation and Analysis of Heritage Timber Roof Structures," in *Digital Heritage. Progress in Cultural Heritage: Documentation, Preservation, and Protection*, M. Ioannides,

- E. Fink, A. Moropoulou, M. Hagedorn-Saupe, A. Fresa, G. Liestøl, V. Rajcic, and P. Grussenmeyer, Eds., Cham: Springer International Publishing, pp. 79–90.
- [35] P. Crespi *et al.* (2015) “From BIM to FEM: the analysis of an historical masonry building,” in *Building Information Modelling (BIM) in Design, Construction and Operations*, doi: 10.2495/bim150471.
- [36] J. M. López Medina (1995) “El agua en el sureste peninsular durante época romana: su aprovechamiento para la agricultura.,” in *Agricultura y regadío en Al-Andalus, síntesis y problemas: actas del coloquio*, pp. 13–16.
- [37] A. Gil Albarracín (1983) *Construcciones romanas de Almería*. Faventia.
- [38] J. M. Rodríguez López and L. Cara Barrionuevo (1989) “Aproximación al conocimiento de la historia agrícola de la Alpujarra oriental (Almería): épocas antigua y medieval,” *El agua en zonas áridas. Arqueología e historia. Hidráulica tradicional de la provincia de Almería. Instituto de Estudios Almerienses*, pp. 441–446.
- [39] J. P. Vázquez Guzmán (2014) “La hidráulica rural de Carcauz (Vicar-Almería),” *Revista de Hespérides*, vol. 16, pp. 7–10.
- [40] C. de C. y P. H. Andalucía (2022) *Resolución de 17 de junio de 2022, de la Delegación Territorial de Cultura y Patrimonio Histórico en Almería, por la que se incoa el procedimiento para la inscripción, en el Catálogo General del Patrimonio Histórico Andaluz, como Bien de Interés Cultural* [Online] Available: <https://www.juntadeandalucia.es/boja/2022/119/32#descargas>
- [41] F. Agüera-Vega, F. Carvajal-Ramírez, and P. Martínez-Carricondo (2017) “Assessment of photogrammetric mapping accuracy based on variation ground control points number using unmanned aerial vehicle,” *Measurement*, vol. 98, pp. 221–227, doi: 10.1016/j.measurement.2016.12.002.
- [42] T. Rosnell and E. Honkavaara (2012) “Point cloud generation from aerial image data acquired by a quadcopter type micro unmanned aerial vehicle and a digital still camera,” *Sensors*, vol. 12, no. 1, pp. 453–480, doi: 10.3390/s120100453.
- [43] S. Ochmann, R. Vock, and R. Klein (2019) “Automatic reconstruction of fully volumetric 3D building models from oriented point clouds,” *ISPRS Journal of Photogrammetry and Remote Sensing*, vol. 151, pp. 251–262, doi: 10.1016/j.isprs.2019.03.017.
- [44] C. Dore and M. Murphy (2012) “Integration of Historic Building Information Modeling (HBIM) and 3D GIS for recording and managing cultural heritage sites,” *Proceedings of the 2012 18th International Conference on Virtual Systems and Multimedia, VSMM 2012: Virtual Systems in the Information Society*, pp. 369–376, doi: 10.1109/VSMM.2012.6365947.
- [45] F. Chiabrando, M. Lo Turco, and F. Rinaudo (2017) “Modeling decay in an HBIM starting from 3D point clouds. A followed approach for cultural heritage knowledge,” *ISPRS - International Archives of the Photogrammetry, Remote Sensing and Spatial Information Sciences*, vol. XLII-2/W5, pp. 605–612, Aug. 2017, doi: 10.5194/isprs-archives-XLII-2-W5-605-2017.
- [46] D. Girardeau-Montaut (2017) “CloudCompare.” [Online] Available: <http://www.danielgm.net/cc/>
- [47] A. Adami, B. Scala, and A. Spezzoni (2017) “Modelling and accuracy in a BIM environment for planned conservation: The apartment of Troia of Giulio Romano,” *The International Archives of the Photogrammetry, Remote Sensing and Spatial Information Sciences*, vol. XLII-2/W3, pp. 17–23, Feb. 2017, doi: 10.5194/isprs-archives-XLII-2-W3-17-2017.

- [48] P. Martínez-Carricondo, F. Carvajal-Ramírez, L. Yero-Paneque, and F. Agüera-Vega (2019) "Combination of nadiral and oblique UAV photogrammetry and HBIM for the virtual reconstruction of cultural heritage. Case study of Cortijo del Fraile in Níjar, Almería (Spain)," *Building Research and Information*, vol. 48, no. 2, pp. 140–159, doi: 10.1080/09613218.2019.1626213.
- [49] J. A. Martín Caro (2001) *Análisis estructural de puentes arco de fábrica: Criterios de comprobación*, ACHE.
- [50] C. Jofré-briceño, F. M. La Rivera, E. Atencio, and R. F. Herrera (2021) "Implementation of facility management for port infrastructure through the use of uavs, photogrammetry and bim," *Sensors*, vol. 21, no. 19, doi: 10.3390/s21196686.
- [51] C. Rizo-Maestre, Á. González-Avilés, A. Galiano-Garrigós, M. D. Andújar-Montoya, and J. A. Puchol-García (2020) "UAV + BIM: Incorporation of photogrammetric techniques in architectural projects with building information modeling versus classical work processes," *Remote Sens (Basel)*, vol. 12, no. 14, doi: 10.3390/rs12142329.
- [52] A. Braun and A. Borrmann (2019) "Combining inverse photogrammetry and BIM for automated labeling of construction site images for machine learning," *Autom Constr*, vol. 106, doi: 10.1016/j.autcon.2019.102879.
- [53] M. Faltýnová, E. Matoušková, J. Šedina, and K. Pavelka (2016) "BUILDING FACADE DOCUMENTATION USING LASER SCANNING AND PHOTOGRAMMETRY AND DATA IMPLEMENTATION INTO BIM," *The International Archives of the Photogrammetry, Remote Sensing and Spatial Information Sciences*, vol. XLI-B3, doi: 10.5194/isprs-archives-xli-b3-215-2016.
- [54] F. Clapuyt, V. Vanacker, and K. Van Oost (2016) "Reproducibility of UAV-based earth topography reconstructions based on Structure-from-Motion algorithms," *Geomorphology*, vol. 260, pp. 4–15, doi: 10.1016/j.geomorph.2015.05.011.
- [55] I. Aicardi, F. Chiabrando, N. Grasso, A. M. Lingua, F. Noardo, and A. Spanò (2016) "UAV photogrammetry with oblique images: first analysis on data acquisition and processing," *ISPRS - International Archives of the Photogrammetry, Remote Sensing and Spatial Information Sciences*, vol. XLI-B1, pp. 835–842, Jun. 2016, doi: 10.5194/isprsarchives-XLI-B1-835-2016.
- [56] E. Karachaliou, E. Georgiou, D. Psaltis, and E. Stylianidis (2019) "UAV for mapping historic buildings: from 3D modelling to BIM," *ISPRS - International Archives of the Photogrammetry, Remote Sensing and Spatial Information Sciences*, vol. XLII-2/W9, pp. 397–402, doi: 10.5194/isprs-archives-xlii-2-w9-397-2019.
- [57] M. Sazzad, S. Azad, T. Islam, and F. Ibna Rahman (2017) "Effect of Mesh Size of Floor Slab against Lateral Loads while using Etabs Program".
- [58] A. Ghavidel, S. R. Mousavi, and M. Rashki (2018) "The effect of FEM mesh density on the failure probability analysis of structures," *KSCE Journal of Civil Engineering*, vol. 22, no. 7, doi: 10.1007/s12205-017-1437-5.
- [59] F. Beirnaert and A. Lippens (2018) "Analysis of the interoperability from BIM to FEM," *Tampere university*, no. May 2018.
- [60] A. S. Birkemo, S. C. Hjortland, and S. M. S. M. K. Samarakoon (2019) "Improvements for the workflow interoperability between bim and fem tools," in *WIT Transactions on the Built Environment*, doi: 10.2495/BIM190271.

## Biographical notes

**José Manuel Casimiro Bernárdez** holds a degree in Civil Engineering from the University of Granada (Spain). He furthered his studies in the field of seismic-resistant design of structures thanks to an exchange scholarship at the Pontificia Universidad Católica de Valparaíso (Chile) in 2014. Throughout the last 10 years he has dedicated himself mainly to structural design, both for buildings and bridges, as part of the company HL Ingeniería de Estructuras together with his partner José Lavado. In 2022 he obtained a Master's degree in Representation and Design in Engineering and Architecture at the University of Almeria (Spain), which has allowed him to progress in Cloud to BIM to FEM research and to carry out the present analysis. In addition, he currently works as a teacher in training cycles where he teaches subjects related to the structural support of tunnels and geotechnical works, among others.

**Patricio Jesús Martínez Carricondo** began his studies in Civil Engineering in the academic year 1997-98 at the ETSICCP in Granada. From January 2004 to July 2011 he worked on different engineering projects of great importance developed in Spain (urbanization, roads, highways, dams, pipelines, etc.). At the end of 2011 he began a Master in Representation and Design in Engineering and Architecture taught, among others, at the University of Almeria. This marked the beginning of a new stage that led to the completion of a doctoral thesis on the application of photogrammetric techniques with drones. At present, his professional activity is dedicated to teaching, as a professor in the area of Graphic Expression in Engineering, doing research and providing services with drones through the Drone R&D Service of the University of Almeria (Spain).

**Francisco Agüera Vega** is a PhD in Agricultural Engineering and full professor in the Engineering Department of the University of Almeria, Spain. Since 2009 he has been working with RPAS as platforms carrying different types of sensors. His research topics include land use analysis, precision agriculture, image classification techniques, photogrammetry, generation and exploitation of digital terrain models. He has been principal researcher in several projects related to these topics. In addition, he has participated in several projects related to the optimization of agricultural machinery inside greenhouses, and applications of RPAS in agriculture. In 2007 he spent time at the Department of Earth Science and Engineering, Imperial College London, United Kingdom, in the Remote Sensing and GIS group, and in 2019 at the Dipartimento di Ingegneria "Enzo Ferrari", Laboratorio di Geomatica, at the Faculty of Engineering, at the Università degli Studi di Modena e Reggio Emilia, Italy. He has published numerous teaching and scientific publications in high impact journals.

**Fernando Carvajal Ramírez** has been a PhD in Agricultural Engineering and Full Professor of the Department of Engineering at the University of Almeria since 2019. As part of his research work, he has published books and scientific journals of impact and has obtained 2 national awards for entrepreneurial initiatives; he has participated in numerous research projects; is editor of an international scientific journal of maximum impact. His teaching received 'excellent' in the DOCENTIA programme accreditation, and the Rectoral Mention of Teaching Excellence. He has published several teaching publications, and has participated in teaching innovation projects, most of them as principal investigator. In terms of didactic management, he is currently Vice-Rector for Post-graduate Studies and Institutional Relations in the University of Almeria (Spain).

## Summary

The Twenty Eyes Aqueduct stands as a monumental hydraulic structure with a rich history spanning several centuries, poised to be designated as a heritage asset of cultural interest (Bien de Interés Cultural, BIC). This infrastructure poses a significant challenge for structural simulation, given the heterogeneous nature of its materials, geometric irregularities and challenging accessibility. Recent advancements in UAV photogrammetry, coupled with the evolution of BIM and the computational capabilities of modern computers for calculating FEM, present a methodology for simulating the behaviour of structures under applied loads. This approach enables us to address the tasks of reconstruction, protection and conservation of our heritage with unprecedented precision, speed and perspective. In this study, the innovative Cloud-to-BIM-to-FEM methodology is applied, which is capable of converting BIM models generated from point clouds into FEM. Obtaining the point cloud was possible using UAV photogrammetry, during which a 3D survey of the current state of the aqueduct was conducted. The point cloud obtained served as the basis for generating an HBIM that accurately represents the geometry of the aqueduct (Cloud-to-BIM). The HBIM was then transformed into a FEM model that respects the monument's singularity without excessive geometric simplifications (BIM-to-FEM). Finally, various considerations were deduced regarding the stability of the aqueduct and its structural behaviour by applying loads such as wind and earthquake.

## Riassunto

L'Acquedotto dei Venti Occhi è una struttura idraulica monumentale con una ricca storia che abbraccia diversi secoli, pronta per essere designata come bene patrimoniale di interesse culturale (Bien de Interés Cultural, BIC). Questa infrastruttura rappresenta una sfida significativa per la simulazione strutturale, data la natura eterogenea dei suoi materiali, le irregolarità geometriche e l'accessibilità difficile. I recenti progressi nella fotogrammetria UAV, insieme all'evoluzione del BIM e alle capacità computazionali dei moderni computer per il calcolo FEM, presentano una metodologia per simulare il comportamento delle strutture sotto carichi applicati. Questo approccio ci consente di affrontare i compiti di ricostruzione, protezione e conservazione del nostro patrimonio con precisione, velocità e prospettiva senza precedenti. In questo studio viene applicata l'innovativa metodologia Cloud-to-BIM-to-FEM, in grado di convertire modelli BIM generati da nuvole di punti in FEM. L'ottenimento della nuvola di punti è stato possibile utilizzando la fotogrammetria UAV, durante la quale è stato condotto un rilievo 3D dello stato attuale dell'acquedotto. La nuvola di punti ottenuta è servita come base per generare un HBIM che rappresenti accuratamente la geometria dell'acquedotto (Cloud-to-BIM). L'HBIM è stato poi trasformato in un modello FEM che rispetta la singolarità del monumento senza eccessive semplificazioni geometriche (BIM-to-FEM). Infine, sono state dedotte diverse considerazioni riguardanti la stabilità dell'acquedotto e il suo comportamento strutturale all'applicazione di carichi quali vento e sisma.